Nanoscale

PAPER

View Article Online
View Journal | View Issue

Cite this: *Nanoscale*, 2018, **10**, 14763

Pulling lipid tubes from supported bilayers unveils the underlying substrate contribution to the membrane mechanics†

Berta Gumí-Audenis,[a,b,c] Luca Costa,[d] Lidia Ferrer-Tasies,[c,e] Imma Ratera,[c,e] Nora Ventosa,[c,e] Fausto Sanz[a,b,c] and Marina I. Giannotti *[a,b,c]

Cell processes like endocytosis, membrane resealing, signaling and transcription involve conformational changes which depend on the chemical composition and the physicochemical properties of the lipid membrane. The better understanding of the mechanical role of lipids in cell membrane force-triggered and sensing mechanisms has recently become the focus of attention. Different membrane models and experimental methodologies are commonly explored. While general approaches involve controlled vesicle deformation using micropipettes or optical tweezers, due to the local and dynamic nature of the membrane, high spatial resolution atomic force microscopy (AFM) has been widely used to study the mechanical compression and indentation of supported lipid bilayers (SLBs). However, the substrate contribution remains unkown. Here, we demonstrate how pulling lipid tubes with an AFM out of model SLBs can be used to assess the nanomechanics of SLBs through the evaluation of the tube growing force (F_{tube}), allowing for very local evaluation with high spatial and force resolution of the lipid membrane tension. We first validate this approach to determine the contribution of different phospholipids, by varying the membrane composition, in both one-component and phase-segregated membranes. Finally, we successfully assess the contribution of the underlying substrate to the membrane mechanics, demonstrating that SLB models may represent an intermediate scenario between a free membrane (blebs) and a cytoskeleton supported membrane.

Received 20th April 2018,
Accepted 11th July 2018

DOI: 10.1039/c8nr03249a

rsc.li/nanoscale

Introduction

Several cellular processes, including adhesion, endocytosis, membrane resealing, signaling and transcription, among others, involve conformational changes such as bending, vesiculation and tubulation.[1,2] For instance, in endocytosis, the endocytic system needs to generate force enough to form an endocytic vesicle by bending the membrane bilayer.[3] A biological process in which membrane tubes or tethers are formed occurs during neutrophil rolling along the endothelium and adhesion to platelets.[4,5] Separation of a membrane segment from the cytoskeleton as well as strong membrane bending are both involved in these mechanisms, for which the membrane chemical composition and physicochemical properties are key players,[1] often highly localized and dynamic.[6]

The mechanical role of the lipid membrane in force triggered (or sensing) mechanisms in cells is being paid increasing attention, in addition to the more established role of the mechanosensitive proteins. Studies on the mechanical properties of model membranes have shown that subtle changes in the membrane chemical composition affect the overall mechanical response. Micropipette aspiration is one of the most used techniques to evaluate the elasticity of giant unilamellar vesicles (GUVs) at the mesoscopic scale.[7–9] Still, the heterogeneity of biological membranes, with domains at the micro and nanoscales, led to focus on nanometric resolution techniques like atomic force microscopy (AFM), specifically force spectroscopy (FS), to study supported lipid bilayers (SLBs).[10–15] In these experiments, the tip of the AFM cantilever

[a]*Institute for Bioengineering of Catalonia (IBEC), The Barcelona Institute of Science and Technology (BIST), Baldiri Reixac 10–12, 08028 Barcelona, Spain. E-mail: migiannotti@ibecbarcelona.eu*
[b]*Department of Material Science and Physical Chemistry, University of Barcelona, Martí i Franquès 1-11, 08028 Barcelona, Spain*
[c]*Centro de Investigación Biomédica en Red (CIBER), Instituto de Salud Carlos III, Monforte de Lemos 3-5, 28029 Madrid, Spain*
[d]*Centre de Biochimie Structurale (CBS), CNRS UMR 5048 – UM – INSERM U 1054, 60 rue de Navacelles, 34090 Montpellier, France*
[e]*Institut de Ciència de Materials de Barcelona (ICMAB-CSIC), Campus Universitari de Bellaterra, 08193 Cerdanyola del Vallès, Spain*

†Electronic supplementary information (ESI) available: Breakthrough force (F_b) values for different membrane chemical compositions. F_{tube} histograms for DOPC and DSPC SLBs at different tip retracting velocities. DOPC on PEG-grafted-mica preliminary studies. See DOI: 10.1039/c8nr03249a

is typically used to sense and apply force, penetrating an individual SLB. The vertical force required to break through the bilayer, the breakthrough force (F_b), is usually in the order of several nN and is considered as a direct measurement of the local lateral interactions between lipid molecules. Using the F_b approach it has been demonstrated how the membrane mechanics is significantly altered by subtle variations in the chemical composition[16,17] and the physicochemical environment (temperature, pH, or ionic strength).[12,16,18–21] It has been shown to be able to resolve very precisely the local mechanical properties in phase segregated membranes.[13,20,22–25]

Still, the real contribution of the underlying rigid substrate on the measured mechanical properties remains unknown, and the SLBs are questioned as representative models of biological membranes. Besides, the membrane being confined to two dimensions prevents from evaluating the intrinsic curvature of the membrane.[26] Minimizing the contribution from the stiff support has been achieved by using alternative models like the pore spanning bilayers on porous substrates,[27–30] the polymer-cushioned membranes[31,32] and the stacked bilayers (or multibilayers).[33–36] Therefore, it is of great interest to assess the substrate effect on the membrane mechanics, and situate the SLB models with respect to their biological counterparts.

Pulling lipids from cells and membranes with a probe (a bead in an optical trap or an AFM tip) by applying a force in the orthogonal direction away from the membrane[37–42] resembles the cell vesiculation and tubulation. It has been reported that in a cell, the tube growing force (F_{tube}) depends on the membrane bending stiffness (κ), the in-plane membrane tension (σ) and the membrane-cytoskeleton adhesion.[3] In regions where the membrane has separated from the cytoskeleton, which is named bleb or free membrane, F_{tube} is strictly dependent on the membrane properties, with the principal contributions being κ and σ, as there is no direct interaction with the cytoskeleton.[43] In general, however, the cytoskeleton adhesion and σ are difficult terms to separate, so it has been designated the so-called apparent membrane tension (σ_{app}), which is defined as the membrane tension when considering the whole cell membrane and taking into account the adhesion contribution (eqn (1)).[3] Hence, variations in the cytoskeleton-membrane adhesion term have a direct impact on the F_{tube}.[43,44]

To relate these membrane parameters, the following mathematical expression (eqn (2)) has been proposed, which is valid when the tube growth occurs under thermodynamic equilibrium, that is in the limit of zero velocity (static thermodynamic analysis):[37–41,45,46]

$$\sigma_{app} = \sigma + \gamma \quad (1)$$

$$\sigma_{app} = \frac{F_{tube}^2}{8\kappa\pi^2} \quad (2)$$

where γ is the adhesion energy parameter.

A simplified but analogous situation occurs when lipid tubes are pulled by an AFM tip from an SLB.[40,41] As exemplified in Fig. 1, during an AFM-FS measurement on an SLB, the AFM tip is approached and retracted from the bilayer at a constant velocity to obtain a register of the force as a function of the tip–sample separation (red dotted curve: approach; blue curve: retract). Once in contact, the AFM tip first compresses the bilayer and finally pierces it in a sudden event at F_b. When retracting from the surface, the tip remains connected to the surface through a lipid tube that grows longer while the tip moves further away up to a certain distance when it breaks and the cantilever returns to the equilibrium position. This process of growing the lipid tube occurs at constant force F_{tube} and it is observed in the retract force-separation curve as a force plateau, at several tens of pN (Fig. 1, blue curve). Yet, from these experiments it is not possible to discern whether both leaflets of the bilayer equally contribute to the tube growth.

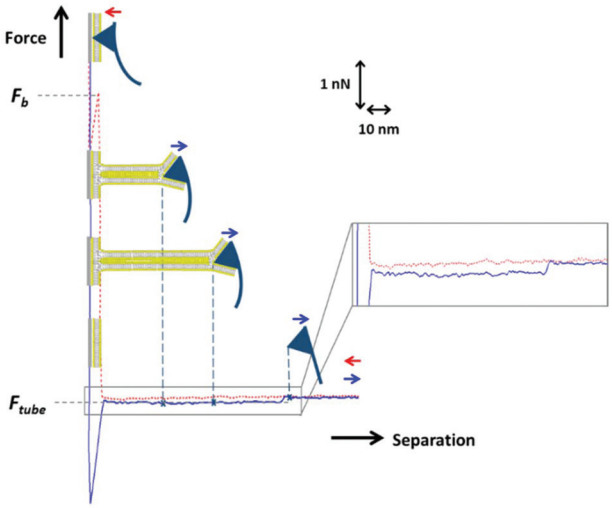

Fig. 1 Force-separation curve when performing an AFM-FS measurement on an SLB: approach (red dotted line) and retract (blue line), showing the breakthrough event and force (F_b) and the tube growing event and force (F_{tube}). Schematic representation of the different steps.

Here, we assess the contribution of the underlying substrate to the membrane mechanics using the AFM to pull membrane tubes from SLBs. We explore the local nanomechanical properties of lipid membranes through the evaluation of the F_{tube} in a lipid tubing force spectroscopy approach, combining the advantage of the AFM to locally probe a sample with lateral resolution at the nanoscale and apply and sense forces in the pN range with the simplicity of the SLB preparation. We validate this approach by assessing the contribution of the chemical composition to the membrane mechanics and we demonstrate its capacity to differentiate domains of different compositions in phase-segregated membranes.

Experimental section

Materials

1,2-Dioleoyl-*sn-glycero*-3-phosphoethanolamine (DOPE, transition temperature, T_m = −16 °C), 1,2-dipalmitoyl-*sn-glycero*-3-

phosphoethanolamine (DPPE, transition temperature (T_m) = 63 °C), 1,2-dioleoyl-*sn-glycero*-3-phosphocholine (DOPC, T_m = −17 °C), 1,2-dipalmitoyl-*sn-glycero*-3-phosphocholine (DPPC, T_m = 41 °C), 1,2-distearoyl-*sn-glycero*-3-phosphocholine (DSPC, T_m = 55 °C), 1,2-dielaidoyl-*sn-glycero*-3-phospho-(1′-*rac*-glycerol) (DOPG, T_m = −18 °C), 1,2-dipalmitoyl-*sn-glycero*-3-phospho-(1′-*rac*-glycerol) (DPPG, T_m = 41 °C) and cholesterol (Chol) were purchased from Sigma-Aldrich (St Louis, MO). The experiments were performed in 150 mM NaCl, 20 mM $MgCl_2$, 20 mM HEPES (4-(2-hydroxyethyl)-1-piperazineethanesulfonic acid) (pH 7.4) buffer or in 94 mM NaCl, 4 mM phosphate saline buffer (PBS) of pH 7.4. Both buffers were prepared with ultrapure water (Milli-Q reverse osmosis system, 18.2 mΩ cm resistivity) and filtered before use with an inorganic membrane filter (0.22 μm pore size Whatman International Ltd, England, UK).

Sample preparation

The different lipids were individually dissolved in chloroform : methanol (v : v 3 : 1) to give a final concentration of 3 mM. Aliquots of each phospholipid, or the corresponding mixture, were poured into a falcon tube, followed by evaporating the solvent to dryness under a nitrogen flow to achieve a thin film spread on the walls of the tube. The dried lipid films were then hydrated with buffer solution (150 mM NaCl, 20 mM $MgCl_2$, 20 mM HEPES, pH 7.4) previously heated above the T_m of the phospholipid, until a final total concentration of 0.5 mM. The falcon tubes were later subjected to cycles of vortex mixing and heating to above the T_m. The vesicle suspensions were placed in an ultrasound bath for 30 min to finally obtain unilamellar vesicles.[22] The DOPC : Chol (80 : 20 molar ratio) vesicles were synthesized by the DELOS-SUSP method[47] and suspended in 94 mM NaCl and 4 mM PBS (pH 7.4).

Supported lipid bilayers (SLBs) were obtained by the vesicle fusion method.[12,48] The vesicle suspensions were deposited onto freshly cleaved circular mica surfaces (Ted Pella, Redding, CA) and incubated for 30 min at a temperature above the phospholipid T_m. After that, the samples were rinsed several times with buffer solution to eliminate unfused vesicles, always keeping the substrates hydrated.

To study supported unfused vesicles, DOPC : Chol vesicles of 70 nm average diameter (and a polydispersity index of 0.2) – from dynamic light scattering (DLS) – were used. Vesicles were deposited onto square silicon substrates with their native oxide (Ted Pella, Redding, CA) previously cleaned with Piranha solution (7 : 3 H_2SO_4 : H_2O_2 (30%). *Caution*: Piranha solution should be handled with extreme care), incubated for 5 min at room temperature (RT) and then rinsed with the corresponding buffer solution. In this case, we obtained a combination of unfused vesicles with some bilayer patches onto the silicon substrate. Only several solid-supported vesicles were analysed, so the size distribution of the vesicles in the suspension may not represent the studied population. Therefore, we measured the size of each individual studied vesicle from the AFM images. When deposited on a surface, the vesicles adopt a spherical cap shape. We obtained an average width (±SD) of the spherical cap of 193 ± 76 nm.

Atomic force microscopy-based force spectroscopy (AFM-FS)

AFM-FS measurements were performed using an MFP-3D AFM (Asylum Research, Santa Barbara, CA) at RT and under liquid conditions (buffer solution), on a sample region previously visualized using AC-mode for SLBs and contact mode for supported vesicles. We used V-shaped Si_3N_4 cantilevers (Bruker AFM Probes, Camarillo, CA) having a nominal spring constant of 0.35 N m^{-1}: SNL, with the tip made of silicon and a nominal tip radius (r_{tip}) between 2 and 12 nm; and DNP, with the tip made of silicon nitride and a nominal r_{tip} between 20 and 60 nm. After having measured the sensitivity (V m^{-1}), the cantilever spring constants were individually calibrated by using the equipartition theorem (thermal noise routine).[49,50] Force–distance curves were recorded by approaching and retracting the AFM tip at 1 μm s^{-1} (unless specifically stated) and in the force map mode. The number of force–distance curves analysed for each system are listed in each figure caption and these correspond to 2 to 3 independent experiments. All F_{tube} and F_b values reported correspond to mean ± SD, unless specifically stated.

Results and discussion

Membrane chemical composition

To demonstrate the power of the lipid tubing force spectroscopy approach, we first assessed the contribution of the membrane composition to the F_{tube}.

One component SLBs. We first assessed the role of the lipid molecular structure in the tube growth process. We prepared and studied SLBs on mica, composed of different individual phospholipids, namely DOPC, DPPC, DOPE, DPPE, DOPG and DPPG. We chose phospholipids of constant chain lengths of 18 (with 1 unsaturation, DO-) and 16 (fully saturated, DP-) C, in fluid and the gel state at room temperature (RT), respectively, while varying the headgroup (phosphoethanolamine (PE), phosphocholine (PC) and phosphoglycerol (PG)) (Fig. 2).

After imaging the samples to locate bilayer patches, force–distance curves were recorded using sharp AFM tips (silicon, nominal tip radius (r_{tip}) between 2 and 12 nm). From the plateaus observed in the retract curves, the F_{tube} values and the distance at which the tubes rupture or detach (d) were obtained. Fig. 2 shows the F_{tube} *vs.* d plots, the F_{tube} and d distributions (a–c) and the F_{tube} mean values (d) for each SLB, sorted by the headgroup.

The tube growing force F_{tube} is lower for liquid-disordered (l_d) bilayers (in the range of 65–80 pN) than for solid-ordered (s_o) bilayers of the same headgroup (in the range of 90–110 pN). While in the l_d state the F_{tube} slightly augments from PE to PC (66 ± 15 pN for DOPE, 80 ± 25 pN for DOPC and 75 ± 13 pN for DOPG), and it clearly increases when changing the headgroup for s_o membranes from PE to PC and then PG (92 ± 20 pN for DPPE, 104 ± 30 pN for DPPC and 112 ± 30 pN for

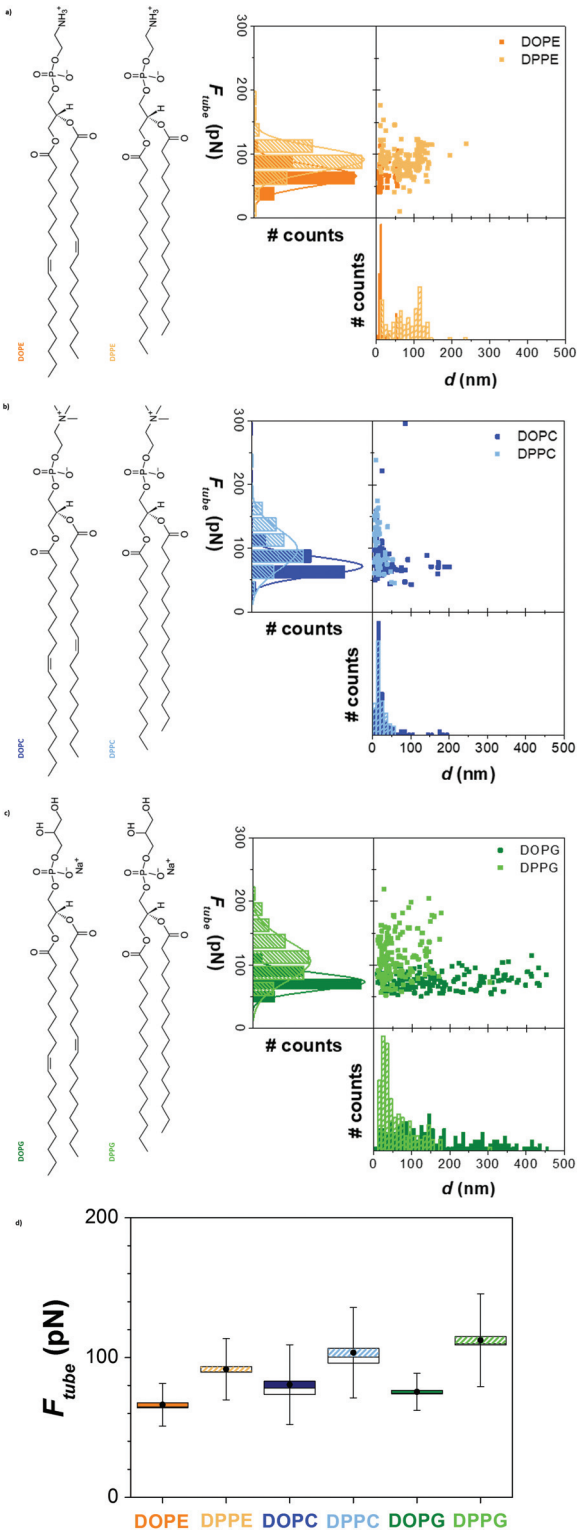

Fig. 2 F_{tube} *vs.* d plots and histograms for all the phospholipid systems sorted by the headgroup: PE (a), PC (b) and PG (c) ($n > 100$), including the phospholipid structures. (d) Boxchart for F_{tube} values showing the mean (●), SE (box) and SD (bars). All the measurements were performed in 150 mM NaCl, 20 mM $MgCl_2$, 20 mM HEPES (pH 7.4) buffer solution and at RT.

DPPG). These values are directly related to the molecular lateral packing and interaction with the substrate and surrounding solvent, mainly of electrostatic nature. Therefore, tube growth from SLBs with the AFM occurs at a higher force for PG SLBs, charged phospholipids that together with the ions from the buffer form strong lateral packing between the lipid headgroups and enhanced interactions with the substrate. This behavior corresponds well with the trend observed in the F_b measured using the approach curves (Fig. S1a†), a well-established characterization methodology for such bilayers.[17,20,22] Not only significantly lower F_b values are obtained for l_d SLBs than for s_o bilayers, but also the values increase following PE < PC < PG (DOPE 3.7 ± 1.6 nN, DPPE 8.9 ± 4.3 nN,[17] DOPC 4.8 ± 0.6 nN, DPPC 16.1 ± 3.4 nN, DOPG 3.8 ± 0.5 nN and DPPG 26.5 ± 3.5 nN). A clear correlation between F_b and F_{tube} is observed (Fig. S1b†).

Interestingly, when increasing the saturated tail length from 16 (DPPC) to 18 (DSPC) C, no significant variation in the F_{tube} (98 ± 12 pN) is observed, with respect to the DPPC bilayers (Fig. S2a and b†). In contrast, this slight difference in the tail length provokes a significant increase in the F_b for DSPC (32.7 ± 2.0 nN) compared to DPPC SLBs (Fig. S2c†).

In general, the distance at which the tubes break or detach from the tip for s_o SLBs extends all over the range up to around 150–200 nm for DPPE (Fig. 2a), with a higher population around 15–40 nm for DPPC and DPPG (Fig. 2b and c). For l_d SLBs, tubes are only pulled to distances below 50 nm, for DOPE and DOPC (Fig. 2a and b). Still, the tubes growing from DOPG bilayers normally extend to much longer distances, reaching values up to 450 nm (Fig. 2a). This might be related to higher ion mediated interactions between the PG lipid molecules and the AFM tip.

From the resultant F_{tube} values, it is possible to estimate the membrane tension, according to eqn (2), when the tube growth can be considered thermodynamically reversible. In our measurements we observed that the F_{tube} did not significantly change with the pulling velocity (1–3 μm s^{-1}) and therefore we assume a quasi-reversible situation. For DOPC, and with κ equal to 17 k_BT obtained from the reported X-ray studies on GUVs,[51] we calculate a σ_{app} of 0.94 pN nm^{-1}. This value agrees with the reported studies performed on DOPC SLBs setting the surface tension and measuring the tube radius.[9,42]

Phase segregated SLBs. Following the same procedure allows us to characterize phase segregated bilayers, and laterally resolve the different domains. To prove this, we studied a mixed bilayer composed of DOPE : DPPG (25 : 75). Vesicles of this composition open on the mica surface to form SLB patches with different domains (Fig. 3a) that correspond to an s_o phase (rich in DPPG) dispersed in an l_d phase (rich in DOPE). When indented by the AFM tip at a constant velocity of 1 μm s^{-1}, a bimodal F_b distribution is obtained (Fig. 3b), with differentiated mean F_b values associated with each domain (5.0 ± 0.6 nN for the lower domain and 11.9 ± 0.9 nN for the thicker one). From the retract force-separation curves, we analyzed those showing the tube pulling event, and obtain an F_{tube} distribution and map (Fig. 3c). The F_{tube} map shows red

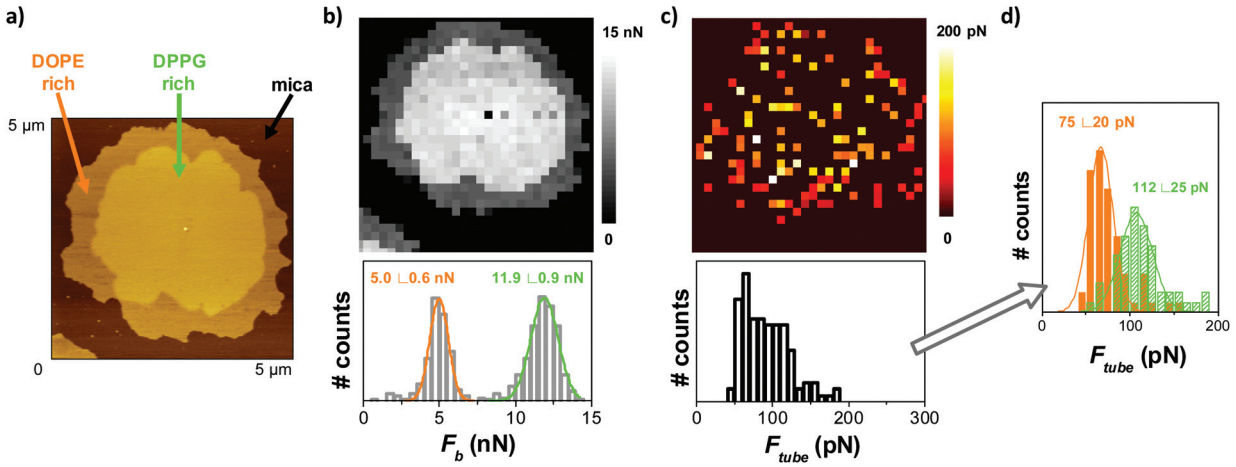

Fig. 3 DOPE : DPPG (25 : 75) SLB on mica: (a) AFM AC mode topographical image, (b) F_b map and distribution, (c) F_{tube} map and distribution (n > 100), and (d) two F_{tube} distributions resolved when separating F_{tube} values according to the corresponding F_b. The experiments were performed in 150 mM NaCl, 20 mM $MgCl_2$, 20 mM HEPES (pH 7.4) buffer solution and at RT.

pixels (lower F_{tube} values) in the region that correspond to the peripheral part of the SLB patch, and yellow pixels (higher F_{tube} values) in the center. When plotted all together, the F_{tube} distribution is wide and corresponds to the convolution of the two distributions, which are resolved when separating them according to the corresponding F_b. Fig. 3d shows two superimposed histograms. The low F_{tube} histogram with a mean value of 75 ± 20 pN (orange) corresponds to the F_{tube} values from the force-separation curves associated with the low F_b (the DOPE-rich phase), while the higher F_{tube} histogram at 112 ± 25 pN (green) corresponds to the F_{tube} from the curves associated with the high F_b (the DPPG-rich phase). F_b and F_{tube} for the domains may differ from the values of pure DOPE and DPPG due to partial miscibility among them. These results demonstrate that pulling tubes from supported membranes allows also the identification of different coexisting domains, providing lateral resolution to the nanomechanical analysis, and demonstrates that segregation of domains may locally tune the mechanical properties of the membranes.

***F_{tube}* does not depend on the AFM tip.** One of the issues when using AFM indentation measurements to determine the elasticity properties of membranes is that the results are highly dependent on the tip size, which needs to be well-characterized, and this is a parameter that can even vary along a study. We study the effect of the AFM tip properties (r_{tip} and tip material) on the F_{tube}. We used two different tips that have the same specifications except for the tip material and its r_{tip}: SNL (Bruker), with a tip made of silicon and nominal r_{tip} between 2 and 12 nm, and DNP (Bruker), with a tip made of silicon nitride and nominal r_{tip} between 20 and 60 nm. We performed the experiments on DOPC bilayers onto mica. The mean F_{tube} value obtained using the sharper (SNL) tips was 80 ± 25 pN, while using blunter (DNP) tips we obtained a mean F_{tube} in the same range: 81 ± 13 pN. Still, we noticed that for higher r_{tip}, more tube growth events were detected in a force map measurement. In any case, we can conclude that even if a bigger r_{tip} may facilitate the tube growth on the tip, it does not modify the resultant F_{tube} value. In studies on cells, a comparable scenario has been observed, where increasing r_{tip} led to the formation of multiple tethers but did not affect the growing force even with different tip functionalization.[52,53]

In general, significant dependence of F_{tube} with the pulling velocity (dynamic contribution) has been reported on lipid vesicles at high pulling velocities (15 to 250 µm s^{-1})[45] and, undoubtedly, on cells,[46,54] attributed to the viscous drag between the monolayers in vesicles, and to the viscous resistance between the membrane and the cytoskeleton in human neutrophils.[46] This has been demonstrated by actin disruption with latrunculin A leading to a dramatic decrease of the effective viscosity to zero (tether forces independent of the pulling rate).[46] In our work on SLBs, however, no variation of the F_{tube} value was observed here when changing the pulling velocity from 1 to 3 µm s^{-1}, tested for DOPC and DSPC bilayers supported onto mica, representative of l_d and s_o SLBs (Fig. S3†). A similar observation has been reported for tubes pulled from SLBs.[55] Therefore, a quasi-static situation for low pulling velocities on SLBs can be considered.

Contribution of the underlying substrate

As previously stated, in regions of a cell where the membrane has separated from the cytoskeleton (blebs), the F_{tube} strictly depends on the membrane bending stiffness κ and the in-plane tension σ.[3] Thus, determining F_{tube} from blebs ($F_{tube\ b}$), where $\gamma = 0$, will allow the separation of adhesion and membrane tension. It has been assessed through measurements from blebs and cytoskeleton supported cell regions ($\gamma \neq 0$) that $F_{tube\ b} < 0.5F_{tube\ cyt}$, meaning that over 75% of that σ_{app} comes from adhesion.[3,43]

In an analogous manner, we assess the adhesion contribution to the membrane apparent tension for a specific support by using eqn (1) and (2), by comparing the F_{tube} of the SLB with that of the same bilayer on a bleb-like situation.

We evaluated the tube growth process from DOPC : Chol (80 : 20 molar ratio) deposited vesicles, where the bilayer is not in direct contact with the substrate. Chol is not only a key player in biological membrane physics, but also involved in liposome pharmacological formulations to tune mechanical properties and permeability.[56] We then compare this result with those obtained for SLBs of the same sample supported on silicon and mica surfaces, as schematized in Fig. 4a. In our experiments, vesicles are analogous to bleb membranes, with $\gamma = 0$ in eqn (1), while the SLBs comprise the adhesion term $\gamma \neq 0$. To study tubing out of vesicles, the deposited vesicles were first localized with contact mode AFM imaging (Fig. 4b) and then force-separation curves were performed on the center of the vesicle.

As shown in the F_{tube} *vs.* d plots with the corresponding distributions and mean F_{tube} values (Fig. 4c and d, respectively), d is equivalent for the three scenarios, with the highest population around 50 nm but reaching values up to 400 nm. On the other hand, the lowest F_{tube} is obtained for the vesicles ($F_{tube\ b}$ = 92 ± 10 pN), shifting to higher F_{tube} values for the SLB on silicon ($F_{tube\ Si}$ = 109 ± 12 pN) and on mica ($F_{tube\ mica}$ = 144 ± 16 pN).

This corresponds to $F_{tube\ Si}$ and $F_{tube\ mica}$ being approximately 15% and 37% higher than $F_{tube\ b}$, respectively (eqn (3) and (4)).

$$F_{tube\ b} = 0.85F_{tube\ Si} \quad (3)$$

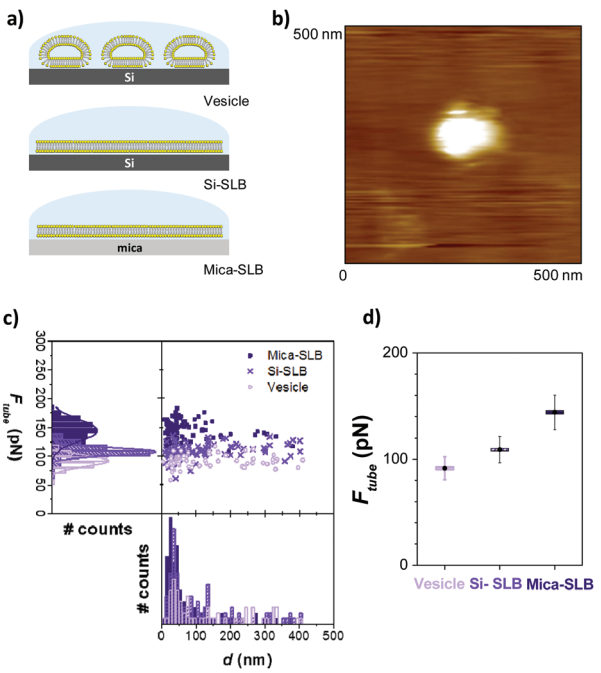

Fig. 4 (a) Scheme of the vesicles deposited onto Si, and the bilayers supported onto Si and mica, for DOPC : Chol (80 : 20 mol ratio). (b) AFM contact mode topographical image of a vesicle onto Si. (c) F_{tube} *vs.* d plots and histograms (n > 65, averaging data from 6 different vesicles), and (d) boxchart for F_{tube} values showing the mean (●), SE (box) and SD (bars), for the 3 situations. The experiments were performed in 94 mM NaCl, 4 mM PBS (pH 7.4) buffer solution and at RT.

$$F_{tube\ b} = 0.63F_{tube\ mica} \quad (4)$$

Combining these results with eqn (1) and (2), we obtain the relationships between the apparent membrane tension for the bleb (σ_b) and each SLB ($\sigma_{app\ Si}$ and $\sigma_{app\ mica}$ for bilayers supported onto silicon or mica, respectively, eqn (5) and (6).

$$\sigma_b = \frac{F_{tube\ b}{}^2}{8\kappa\pi^2} = \frac{(0.85F_{tube\ Si})^2}{8\kappa\pi^2} = 0.72\sigma_{app\ Si} \quad (5)$$

$$\sigma_b = \frac{F_{tube\ b}{}^2}{8\kappa\pi^2} = \frac{(0.63F_{tube\ mica})^2}{8\kappa\pi^2} = 0.40\sigma_{app\ mica} \quad (6)$$

Considering σ_{app} as the sum of σ_b and the corresponding adhesion term γ (eqn (1)), we estimate γ for the SLB onto silicon and mica. For a DOPC : Chol (80 : 20) SLB, γ is approximately 28% and 60% of the apparent membrane tension σ_{app}, on silicon and on mica, respectively. This situates the SLB models as an intermediate scenario between a bleb and a cytoskeleton supported membrane, where over 75% of the apparent membrane tension is believed to come from adhesion.[3] Yet, it is important to take into account that changing the ionic environment or the lipid composition of the membrane, for instance the phospholipid headgroup, would certainly affect the adhesion contribution due to the different electrostatic interaction with the underlying substrate.

It is known that Chol dissolves in the membrane and affects the mechanical properties of fluid-like SLBs, increasing κ.[20,29,57] This allows us to consider for DOPC : Chol (80 : 20) a κ value of 21 k_BT reported for POPC : Chol (75 : 25),[29] higher than that for pure DOPC membranes (17 k_BT), to calculate the in-plane tension for the membrane in the 3 systems. Following eqn (1) and (2) we obtain for the vesicles σ_b = 1.24 pN m^{-1}, for the Si-SLB $\sigma_{app\ Si}$ = 1.71 pN m^{-1}, and for the mica-SLB $\sigma_{app\ mica}$ = 3.08 pN m^{-1}.

The forces measured here for tube extraction from SLBs are, in general, higher than those normally found on cell tethers (20–50 pN), and the lengths of the tubes are considerably shorter.[46,52] This may be related to the strong adhesion energy and in-plane membrane tension with the solid substrates. In agreement, we have observed in preliminary studies on polymer-cushioned membranes, using a PEG-grafted-mica support, that for DOPC SLBs the tube growth occurs at a lower force than on mica (*ca.* 70 pN), but in particular, they grow much longer, with a majority around 500 nm, and extend up to 2 μm (ESI, Fig. S4†). This situation approaches what is generally observed when pulling tethers from cells, where lengths of several microns are usually observed. This methodology may therefore be very useful in the design of the most appropriate substrates and platforms that better mimic the biomembrane arrangement.

Conclusions

We show that pulling lipid tubes from SLBs is valuable to evaluate the mechanical properties of the membrane through measuring the tube growing constant force F_{tube}. This force is

independent of the tip radius and material, in analogy with the force measured by tether pulling AFM experiments performed on living cells.

We first validate the lipid tubing force spectroscopy approach assessing the membrane composition on the mechanics. We demonstrate that the phospholipid state of the SLB determines the tube growing force, which in general is higher for s_o than for l_d bilayers. We show that F_{tube} also depends on the phospholipid headgroup, enhancing F_{tube} values from PE to PC and to PG bilayers, due to stronger interactions between the charged phospholipid headgroups (PG) and the ions from the buffer solution. This behavior is comparable to the one observed in the well-established F_b approach. In contrast to methods that involve micropipettes and optical tweezers, we demonstrate that it is possible to differentiate the local mechanical contribution of different domains in phase-segregated bilayers, with the lateral resolution provided by the AFM and the SLBs, showing that segregation may locally tune the mechanical properties of the membranes. In addition, these measurements complement the characterization upon indentation of the SLBs with the already established F_b procedure, as in one force-separation cycle both sets of data can be recorded.

Most importantly, we evaluated the influence of the underlying substrate on the tube growing force, comparing the tube growth from deposited vesicles and SLBs (on silicon and mica). Following this approach, we were able to assess the contribution of the different substrates on the membrane mechanics, in a specific environment, and we prove that the SLB model represents an intermediate scenario between a free membrane (bleb) and a cytoskeleton supported membrane. This approach contributes to better understand and improve SLBs as models for biomembranes and may assist during the design of cutting-edge substrates and platforms to mimic different circumstances on the cytoskeleton-membrane arrangement.

Conflicts of interest

There are no conflicts to declare.

Acknowledgements

We acknowledge financial support from the Generalitat de Catalunya (AGAUR, 2017 SGR 1442), Spanish Ministry of Economy and Competitiveness (MINECO) and FEDER (CTQ2015-66194-R MINECO/FEDER) and CIBER-BBN (FlexQS-skin) projects, and Instituto de Salud Carlos III, through "Acciones CIBER". The Networking Research Center on Bioengineering, Biomaterials and Nanomedicine (CIBERBBN) is an initiative funded by the VI National R&D&I Plan 2008–2011, Iniciativa Ingenio 2010, Consolider Program, CIBER Actions and financed by the Instituto de Salud Carlos III with assistance from the European Regional Development Fund. We are also grateful to Pau Gorostiza and René Fábregas for fruitful discussions, and to J. Antonio Duran and Blai Barberà for technical assistance.

References

1 G. van Meer, D. R. Voelker and G. W. Feigenson, *Nat. Rev. Mol. Cell Biol.*, 2008, **9**, 112–124.
2 G. van Meer and A. I. P. M. de Kroon, *J. Cell Sci.*, 2011, **124**, 5.
3 M. P. Sheetz, *Nat. Rev. Mol. Cell Biol.*, 2001, **2**, 392.
4 J.-Y. Shao, H. P. Ting-Beall and R. M. Hochmuth, *Proc. Natl. Acad. Sci. U. S. A.*, 1998, **95**, 6797.
5 D. W. Schmidtke and S. L. Diamond, *J. Cell Biol.*, 2000, **149**, 719.
6 E. Lauwers, R. Goodchild and P. Verstreken, *Neuron*, 2016, **90**, 11–25.
7 E. Evans and D. Needham, *J. Phys. Chem.*, 1987, **91**, 4219–4228.
8 M. Saleem, S. Morlot, A. Hohendahl, J. Manzi, M. Lenz and A. Roux, *Nat. Commun.*, 2015, **6**, 6249.
9 W. Rawicz, K. C. Olbrich, T. McIntosh, D. Needham and E. Evans, *Biophys. J.*, 2000, **79**, 328–339.
10 Y. F. Dufrêne and G. U. Lee, *Biochim. Biophys. Acta, Biomembr.*, 2000, **1509**, 14–41.
11 S. Garcia-Manyes and F. Sanz, *Biochim. Biophys. Acta, Biomembr.*, 2010, **1798**, 741–749.
12 L. Redondo-Morata, M. I. Giannotti and F. Sanz, *Mol. Membr. Biol.*, 2014, **31**, 17–28.
13 B. Gumí-Audenis, L. Costa, F. Carlà, F. Comin, F. Sanz and I. M. Giannotti, *Membranes*, 2016, **6**, 58.
14 L. Picas, P.-E. Milhiet and J. Hernández-Borrell, *Chem. Phys. Lipids*, 2012, **165**, 845–860.
15 L. Picas, F. Rico and S. Scheuring, *Biophys. J.*, 2012, **102**, L1–L3.
16 S. Garcia-Manyes, G. Oncins and F. Sanz, *Biophys. J.*, 2005, **89**, 1812–1826.
17 S. Garcia-Manyes, L. Redondo-Morata, G. Oncins and F. Sanz, *J. Am. Chem. Soc.*, 2010, **132**, 12874–12886.
18 S. Garcia-Manyes, G. Oncins and F. Sanz, *Electrochim. Acta*, 2006, **51**, 5029–5036.
19 L. Redondo-Morata, G. Oncins and F. Sanz, *Biophys. J.*, 2012, **102**, 66–74.
20 L. Redondo-Morata, M. I. Giannotti and F. Sanz, *Langmuir*, 2012, **28**, 12851–12860.
21 S. Garcia-Manyes, G. Oncins and F. Sanz, *Biophys. J.*, 2005, **89**, 4261–4274.
22 B. Gumi-Audenis, F. Sanz and M. I. Giannotti, *Soft Matter*, 2015, **11**, 5447–5454.
23 J. K. Li, R. M. A. Sullan and S. Zou, *Langmuir*, 2011, **27**, 1308–1313.
24 M. H. Abdulreda and V. T. Moy, *Biophys. J.*, 2007, **92**, 4369–4378.
25 R. M. A. Sullan, J. K. Li and S. Zou, *Langmuir*, 2009, **25**, 7471–7477.

26 R. Glazier and K. Salaita, *Biochim. Biophys. Acta, Biomembr.*, 2017, **1859**, 1465–1482.
27 B. Lorenz, I. Mey, S. Steltenkamp, T. Fine, C. Rommel, M. M. Müller, A. Maiwald, J. Wegener, C. Steinem and A. Janshoff, *Small*, 2009, **5**, 832–838.
28 I. Mey, M. Stephan, E. K. Schmitt, M. M. Müller, M. Ben Amar, C. Steinem and A. Janshoff, *J. Am. Chem. Soc.*, 2009, **131**, 7031–7039.
29 M. Kocun and A. Janshoff, *Small*, 2012, **8**, 847–851.
30 A. Janshoff and C. Steinem, *Biochim. Biophys. Acta, Mol. Cell Res.*, 2015, **1853**, 2977–2983.
31 M. Tanaka and E. Sackmann, *Nature*, 2005, **437**, 656.
32 J. Andersson and I. Köper, *Membranes*, 2016, **6**, 30.
33 L. Redondo-Morata, M. I. Giannotti and F. Sanz, *Langmuir*, 2012, **28**, 6403–6410.
34 B. D. Almquist and N. A. Melosh, *Nano Lett.*, 2011, **11**, 2066–2070.
35 M. R. Angle, A. Wang, A. Thomas, A. T. Schaefer and N. A. Melosh, *Biophys. J.*, 2014, **107**, 2091–2100.
36 C. Canale, M. Jacono, A. Diaspro and S. Dante, *Microsc. Res. Tech.*, 2010, **73**, 965–972.
37 P. B. Canham, *J. Theor. Biol.*, 1970, **26**, 61–81.
38 J. Daillant, E. Bellet-Amalric, A. Braslau, T. Charitat, G. Fragneto, F. Graner, S. Mora, F. Rieutord and B. Stidder, *Proc. Natl. Acad. Sci. U. S. A.*, 2005, **102**, 11639.
39 R. M. Hochmuth, J. Y. Shao, J. Dai and M. P. Sheetz, *Biophys. J.*, 1996, **70**, 358–369.
40 A. Roux, *Soft Matter*, 2013, **9**, 6726–6736.
41 J. W. Armond, J. V. Macpherson and M. S. Turner, *Langmuir*, 2011, **27**, 8269–8274.
42 I. Pera, R. Stark, M. Kappl, H. J. Butt and F. Benfenati, *Biophys. J.*, 2004, **87**, 2446–2455.
43 J. Dai and M. P. Sheetz, *Biophys. J.*, 1999, **77**, 3363–3370.
44 D. Raucher, T. Stauffer, W. Chen, K. Shen, S. Guo, J. D. York, M. P. Sheetz and T. Meyer, *Cell*, 2000, **100**, 221–228.
45 E. Evans and A. Yeung, *Chem. Phys. Lipids*, 1994, **73**, 39–56.
46 W. D. Marcus and R. M. Hochmuth, *Ann. Biomed. Eng.*, 2002, **30**, 1273–1280.
47 M. Cano-Sarabia, N. Ventosa, S. Sala, C. Patiño, R. Arranz and J. Veciana, *Langmuir*, 2008, **24**, 2433–2437.
48 I. Reviakine and A. Brisson, *Langmuir*, 2000, **16**, 1806–1815.
49 R. Proksch, T. E. Schaffer, J. P. Cleveland, R. C. Callahan and M. B. Viani, *Nanotechnology*, 2004, **15**, 1344–1350.
50 J. L. Hutter and J. Bechhoefer, *Rev. Sci. Instrum.*, 1993, **64**, 1868–1873.
51 J. F. Nagle, M. S. Jablin, S. Tristram-Nagle and K. Akabori, *Chem. Phys. Lipids*, 2015, **185**, 3–10.
52 M. Sun, J. S. Graham, B. Hegedüs, F. Marga, Y. Zhang, G. Forgacs and M. Grandbois, *Biophys. J.*, 2005, **89**, 4320–4329.
53 G. Girdhar and J.-Y. Shao, *Biophys. J.*, 2004, **87**, 3561–3568.
54 F. Brochard-Wyart, N. Borghi, D. Cuvelier and P. Nassoy, *Proc. Natl. Acad. Sci. U. S. A.*, 2006, **103**, 7660.
55 N. Maeda, T. J. Senden and J.-M. di Meglio, *Biochim. Biophys. Acta, Biomembr.*, 2002, **1564**, 165–172.
56 Z. Rukavina and Ž. Vanić, *Pharmaceutics*, 2016, **8**, 18.
57 R. Dimova, *Adv. Colloid Interface Sci.*, 2014, **208**, 225–234.